Annales Geophysicae (2002) 20: 203–212 © European Geophysical Society 2002

Annales Geophysicae

Doppler temperatures from O(^{1}D) airglow in the daytime thermosphere as observed by the Wind Imaging Interferometer (WINDII) on the UARS satellite

C. Lathuillère[1], W. A. Gault[2], B. Lamballais[1], Y. J. Rochon[3], and B. H. Solheim[2]

[1]Laboratoire de Planétologie de Grenoble, CNRS/UJF/OSUG, Batiment D de Physique, BP 53, 38041 Grenoble Cedex 9, France
[2]Centre for Research in Earth and Space Science, York University, 4700 Keele Street, Toronto, Ontario M3J 1P3, Canada
[3]Meteorological Service of Canada, Environment Canada, 4905 Dufferin Street, Toronto, Ontario M3H 5T4, Canada

Received: 21 April 2001 – Accepted: 10 July 2001

Abstract. From 1992 to 1997, the WINDII interferometer on board the UARS satellite acquired a large set of thermospheric data from the O(^{1}D) and O(^{1}S) airglows. We report here for the first time on daytime O(^{1}D) Doppler temperatures obtained with version 5.11 of the WINDII data processing software. Using a statistical analysis of the temperatures independently measured by the two WINDII fields of view, we estimate that the temperature variations larger than 40 K can be considered as geophysical. Comparisons of WINDII temperatures measured during magnetically quiet days with temperatures obtained by the MSIS-90 and DTM-94 thermospheric models show a 100 K bias. We demonstrate, however, that the modeled temperature variations represent very well the mean temperature variation observed by WINDII over 4 years. We also show that the observed latitudinal/local time variation is in very good agreement with the two empirical models. Finally, the temperature variations during a magnetically disturbed day are found to be qualitatively well represented in form by the models, but largely underestimated. The presence of non-thermal atoms and instrument related issues are discussed as possible explanations for the 100 K bias between the WINDII Doppler temperatures and the empirical models.

Key words. Atmospheric composition and structure (airglow and aurora; pressure, density and temperature; instruments and techniques)

1 Introduction

WINDII, the Wind Imaging Interferometer on NASA's Upper Atmosphere Research Satellite (UARS), is a project supported jointly by the Canadian Space Agency and the Centre National d'Etudes Spatiales. It was launched in September 1991 and has performed without major problems since the launch, producing several million complete measurements of the upper atmospheric airglow emissions. It is an imaging Michelson interferometer and it measures winds, temperatures, and emission rates of the observed emissions above the Earth's limb in two fields of view (FOVs), placed at 45° and 135° to the velocity vector. Winds are measured by detecting the Doppler shifts of the emission lines, while Doppler temperatures are obtained from the visibility, or contrast of the interference fringes. The instrument is described by Shepherd et al. (1993). The performance of the instrument over time has been described by Thuillier et al. (1998). Although the wind measurements in the O(^{1}S) and O(^{1}D) emissions have been validated by comparisons with measurements by other instruments (Gault et al., 1996; Thuillier et al., 1996; Lathuillère et al., 1997), the Doppler temperatures have never been validated. The purpose of the present study is to examine several aspects of the WINDII daytime O(^{1}D) temperature measurements to determine what level of confidence to place in them as indicators of atmospheric temperature.

The Doppler temperature retrieval is explained in the first part of the paper and the difficulties are outlined. In the second part of the paper, we compare the temperatures obtained with version 5.11 of the WINDII software from the observations of the two WINDII FOVs and estimate an upper limit on the temperature variations from instrumental causes. WINDII temperatures are then compared to the empirical models MSIS-90 (Hedin, 1991) and DTM-94 (Berger et al., 1998). Solar cycle and latitudinal variations are shown for magnetically quiet days and an example is given of temperature variations observed during a magnetically disturbed day. Finally, we discuss the bias observed between the data and the models.

2 Doppler temperature retrieval

The Doppler temperature is derived from the visibility, V, of the emission line, which can be determined from each set of

Correspondence to: C. Lathuillère
(chantal.lathuillere@obs.ujf-grenoble.fr)

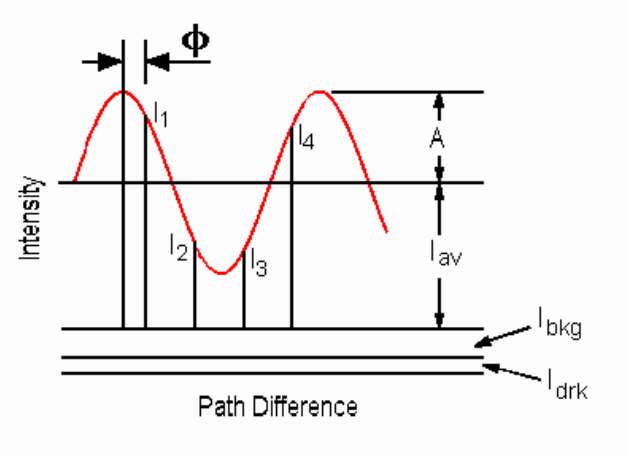

Fig. 1. Intensity vs. path difference for a single fringe, showing the four sampled intensities (I1...I4), the average signal corrected for dark current and background (I_{DB}), the apparent amplitude (A'), the background signal (I_{bkg}), and dark signal (I_{drk}).

measurements. V is defined as the ratio of the fringe amplitude, A, to the average intensity, I_{DB}:

$$V = \frac{A}{I_{DB}}. \quad (1)$$

The equation relating V with temperature, T, assumes a simple emission line produced by atoms in thermal equilibrium with the ambient atmosphere. This assumption has recently been discussed by Shematovitch et al. (1999) and will be examined in Sect. 6. The equation used is:

$$V = e^{-QD^2T}, \quad (2)$$

where Q is a constant equal to $2.87 \times 10^{-5}\,\mathrm{cm^{-2}K^{-1}}$ in the case of the O(^{1}D) emission line, and D is the effective path difference, introduced by Thuillier and Hersé (1991) for the wind calculation. It is shown in the Appendix that this effective path difference must also be used in determining Doppler temperatures, rather than the simple path difference used in the versions of the WINDII software prior to V5.11.

For the O(^{1}D) measurements, WINDII takes four exposures, spaced by $\lambda/4$ in path difference. V can be derived from these four intensities, but first, some corrections must be applied, which include the following in the order given:

(a) dark current (I_{drk}) subtraction,

(b) background (I_{bkg}) subtraction,

(c) correction for transmission variations in the field-of-view at the emission line wavelength, and

(d) instrument visibility correction.

In Fig. 1, a single fringe is shown as a plot of intensity vs. path difference, with the underlying I_{drk} and I_{bkg} components. The dark signal is subtracted by using an interpolated dark current map of the CCD array detector, based on the data from frequent calibrations. The daytime background signal is due to unwanted sunlight, which enters the field-of-view through scattering from clouds, the Earth's surface, and the lower atmosphere. A background measurement is made for each set of emission line measurements by recording one image using a filter centred at 552.5 nm. The background image is multiplied by a single factor B to allow for the different filter bandwidths, solar illumination, etc. and then subtracted from each airglow intensity image. The background conversion factor, B, used in the first versions of the WINDII software, was calculated from the measured transmission profiles and the relative solar intensity at the different wavelengths, but the spectral characteristics of the scattering were unknown and could not be taken into account. This factor, which is a constant defined in the characterization data base for each emission line and each aperture (day and night), was originally overestimated by almost a factor of two for the daytime O(^{1}D) emission. This has resulted in too much background being subtracted, causing the daytime O(^{1}D) intensities to be slightly underestimated. It has also had a large effect on the Doppler temperatures in the earlier versions. A revised estimate for B has been calculated using the premise that the same volume of emission seen in the two FOVs should have the same intensity. But since the common volume is seen from different points on the orbit, the amount of background scattered light is, in general, different in the two fields of view, and this has provided a mean of differentiating between the background and the unmodulated portion of the emission line (Gault et al., 1999). Implicit in this approach is the assumption that subtraction of the measured emission at 552.5 nm scaled by a single factor is sufficient in

Table 1. List of days used to compare the temperatures of the two FOVs. The latitudinal coverage is the part that is common to both FOVs. The two added letters indicate if WINDII was looking northward or southward of the orbital plane (n or s) and if the satellite was travelling northward or southward in its orbit (N or S)

UARS day	Date	Latitudinal coverage		Ap	F10.7 cm (Previous day)
185	14 Mar. 1992	(6;62)	nS	4	163.3
231	29 Apr. 1992	(−36;12)	sN	7	130.4
378	23 Sep. 1992	(−32;27)	nN	9	112.3
490	13 Jan. 1993	(−50;10)	sS	12	135.6
514	06 Feb. 1993	(−62;−15)	sN	5	155.6
532	24 Feb. 1993	(−12;48)	nN	6	129.6
602	05 May 1993	(0;57)	nN	6	112.4
798	17 Nov. 1993	(−63;−39)	sN	6	98.2
805	24 Nov. 1993	(−61;−19)	sN	5	97.9
929	28 Mar. 1994	(−55;−7)	sS	12	88.0
933	01 Apr. 1994	(−65;−45)	sS	6	84.9
1288	22 Mar. 1995	(−51;18)	sS	3	89.0
1386	28 Jun. 1995	(−41;23)	sN	10	74.0

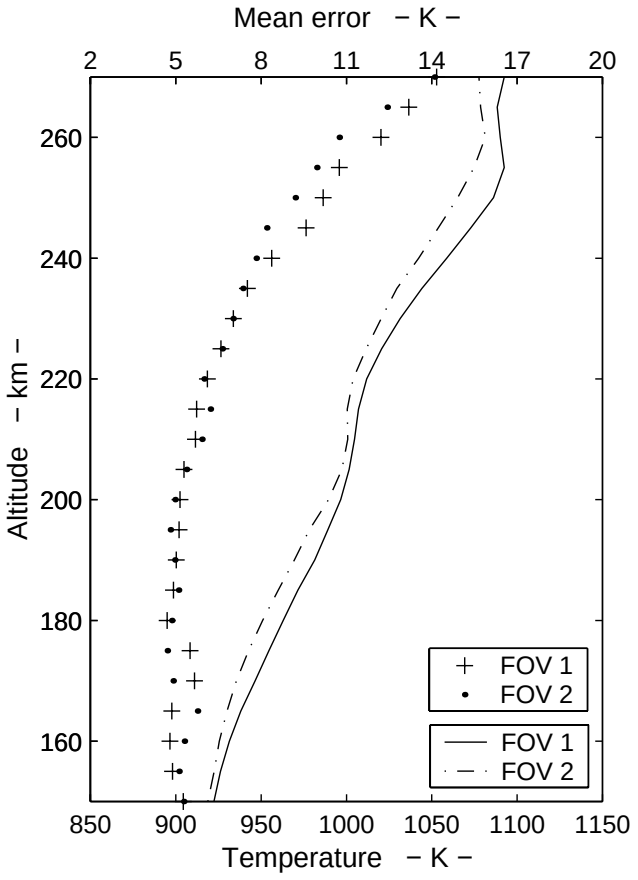

Fig. 2. Mean apparent temperature profiles for the two FOVs on UARS day 378. The mean errors are indicated by dots and crosses, and refer to the upper horizontal scale.

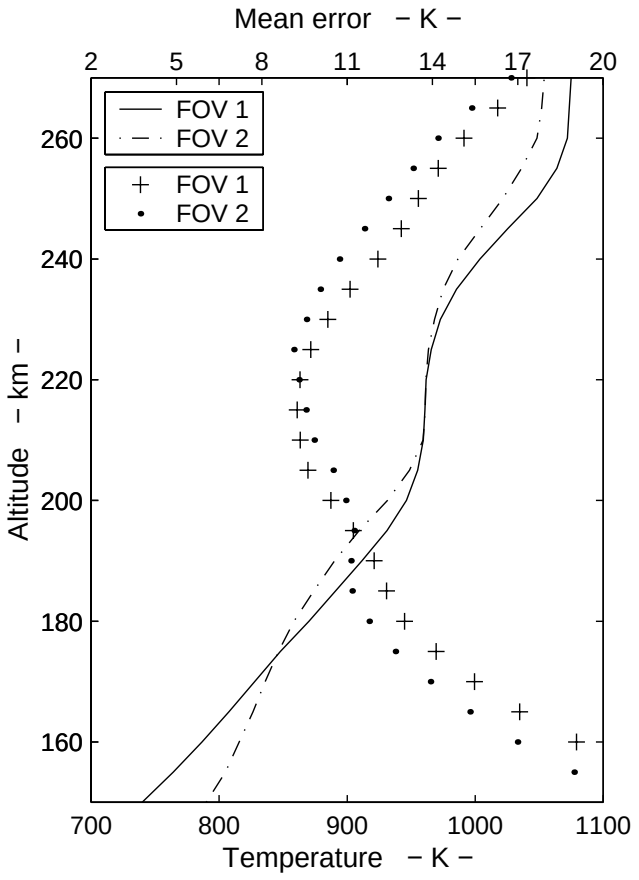

Fig. 3. Mean temperature profiles for the two FOVs on day 378. The mean errors are indicated by dots and crosses, and refer to the upper horizontal scale. They are the smallest around the altitude of the maximum of the O(^{1}D) layer.

removing all, or most of the atmospheric background signal at 630.0 nm.

Once the dark current and the background have been subtracted, the images are divided by the filter transmittance images, measured prior to flight, to allow for the varying transmittance at the wavelength of the emission line. A visibility, $V' = A'/I_{DB}$, is then calculated using the corrected intensities, but this V' is always less than the visibility, V, required in Eq. (2), due to the imperfections in the interferometer. Finally, V is calculated from

$$V = V'/U, \tag{3}$$

where U is the instrument visibility factor, measured in the pre-flight characterization and monitored during the mission using the onboard laser.

The apparent temperatures are obtained from visibility V using Eq. (2). These temperatures correspond to an integration of the emission along the lines-of-sight. The last step consists of the inversion of these apparent quantities to obtain a temperature profile as a function of altitude, as described for wind measurements by Gault et al. (1996). The detailed description of the inversion technique has been given by Rochon (2000).

3 Field-of-view temperature comparison

One of the main problems of the Doppler temperature retrieval, as we have outlined above, is the correct subtraction of the background from the airglow images. The comparison of the results obtained from measurements in the two FOVs, which are analyzed completely independently, provides a way to check a posteriori if the background subtraction is correctly done. We have chosen to study 13 days, distributed over the first 4 years of the UARS mission. These days are identified by their UARS day number (day 1 corresponds to the launch date). Table 1 gives the corresponding dates, as well as the latitudinal coverage of the daytime data. These days have been chosen from the magnetically quiet days for which the O(^{1}D) filter was used, i.e. one day per week or less. The daily A_p index and the value of the F10.7 index, which represent, respectively, the magnetic and solar activity, are also indicated in Table 1.

For each day, we have restricted our analysis either to the part of the orbits when the satellite was travelling north or travelling south, depending on which part had more daytime data. For each orbit and each FOV, apparent temperatures are linearly interpolated in altitude and in latitude. We can then

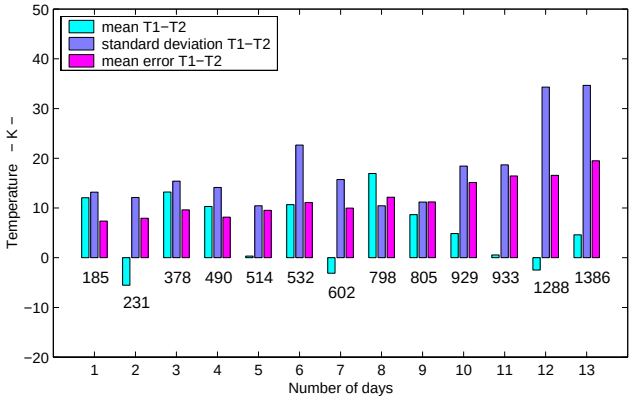

Fig. 4. Mean apparent temperature differences between the two FOVs for 13 days, averaged over the tangent altitude range of 180 to 260 km. The standard deviations of the differences and the mean errors are also indicated.

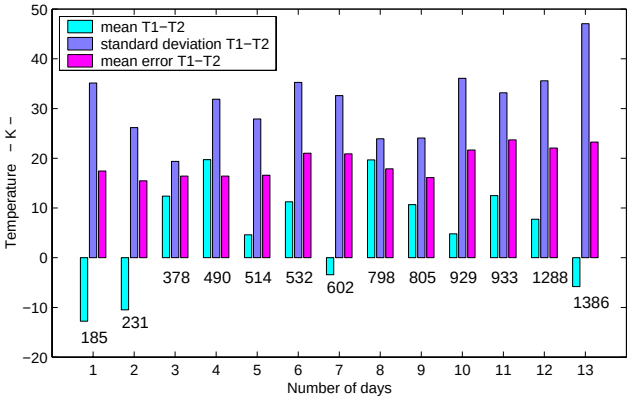

Fig. 5. Mean temperature differences between the two FOVs for 13 days, averaged over the altitude range of 180 to 260 km. The standard deviations of the differences and the mean errors are also indicated.

calculate the temperatures measured at the same tangent altitude and at the same latitude and determine their differences. The same calculations are also performed with inverted temperatures. The time delay between the two measurements is of the order of 8 min, allowing us to assume that the atmosphere is constant.

Figure 2 shows the mean value of the apparent temperature as a function of tangent altitude for day 378 whose latitudinal coverage extends only to mid-latitude (see Table 1). The corresponding latitudinal-local time variation of the temperature is small. For this day, the temperature of FOV1 is larger than or equal to that of FOV2. The amplitude of the temperature difference varies with tangent altitude and can be slightly larger than the measurement error. The variation of the temperature with tangent altitude is typically oscillatory, with amplitude and phase that are variable from one FOV to the other and from one day to another. Figure 3 shows the mean inverted temperature profiles obtained for the same day. The temperature difference between the two FOVs is largest at the highest and lowest altitudes. This difference becomes larger than the mean error of the data below 160 km. This is due to the downward propagation and amplification of the apparent temperature differences by the inversion process. This becomes most significant in the region of weak emission below the altitude of maximum emission. This behaviour is typical, with the oscillations having increased relative to those of the apparent temperatures due to the inversion. Further work is under way to understand these oscillations, which could be related to the limitations in removing all scattered light effects.

In the following, we limit our investigations to the altitude range of 180–260 km that corresponds to 40 km above and below the maximum of the daytime O(^{1}D) emission, and we work with temperatures averaged in altitude.

In Figs. 4 and 5, we show for the 13 days analyzed, the mean daily temperature difference between the two FOVs. Calculations have been done using apparent temperatures in Fig. 4 and inverted temperatures in Fig. 5. Orbits with poor data are manually eliminated. The mean value is taken over the range of altitudes and latitudes used for each day. Figures 4 and 5 also show both the standard deviation and the mean random error of the temperature difference. This error is calculated from each temperature random error, as given by the WINDII software and described in Rochon (2000) and Gault et al. (1996). It does not take into account any potential systematic bias, for example, as the uncertainty in the background factor. The comparison of the mean errors and the standard deviations is an indication of how much of the standard deviation is due to random errors.

Extreme values of the daily apparent temperature difference are 16 K and −7 K. They are a little higher in the case of inverted temperatures: 20 K and −12 K. While the daily temperature differences are smaller than the standard deviation, σ_a, of the individual $T1 - T2$ values and smaller than the mean errors, they are larger than their own standard deviation, σ_m, where $\sigma_m = \sigma_a/\sqrt{N}$, and N is the number of $T1 - T2$ values used to calculate the mean. Since N ranges from approximately 1800 to 5600, the averaged temperature difference between the two FOVs is statistically significant and this difference varies from one day to another in the days that were studied. Although this difference is statistically significant, it is much smaller than prior to correcting the background subtraction factor (versions of the data analysis software prior to V5.11).

A variation of the $T1 - T2$ values could be caused by changes in the instrument visibility factor, U, if they are not accounted for by the weekly visibility calibrations. However, Thuillier, et al. (1998) have shown that U has been remarkably stable over the mission. Their Fig. 5 from the laser calibrations shows a slight increase during the first year, followed by a gradual decrease to day 1900, when their data end. The total variation over this period is about 2%. The small variations around this general trend appear to be of the order of ± 0.1%, corresponding to ± 1.6 K in the ^{1}D emis-

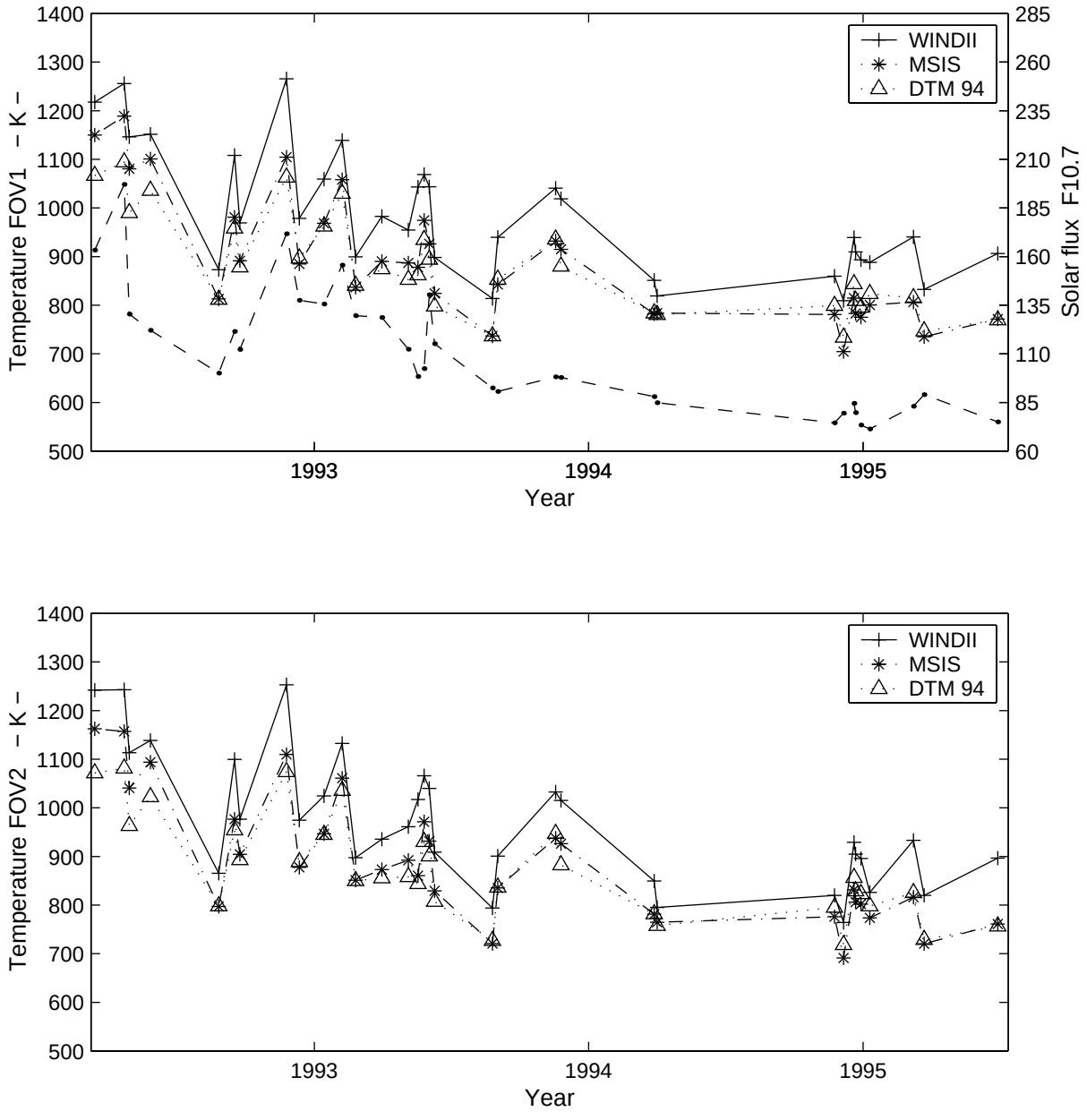

Fig. 6. Mean temperatures averaged over the altitude range of 180 to 260 km for 33 quiet days. The upper and lower panels correspond, respectively, to FOV 1 and 2. WINDII data are plotted with the continuous line, while the temperatures obtained from the MSIS-90 and DTM-94 models are, respectively, plotted with the dash-dotted and the dotted lines. The F10.7 cm index (of the previous day) is shown as a dashed line in the upper panel. The corresponding scale is on the right side of the plot.

sion. The general trend is corrected by regular updates to the characterization data base. The variations about this trend are much too small to be the cause of the changes in $T1 - T2$, as seen in Figs. 4 and 5.

Another possible cause of the changes in $T1 - T2$ is the background subtraction. Unfortunately, the background filter at 552.5 nm is rather far removed from the ^{1}D emission at 630.0 nm, so a change in the average spectral distribution of the scattered background light could affect $T1 - T2$. The background level is, in general, different in the two FOVs, sometimes by as much as a factor of five, so any improperly corrected portion of the background level would affect the two FOVs differently, producing variations in $T1 - T2$. In fact, the background light is probably composed of several components that might behave somewhat differently from each other. The background light will be the subject of further study.

A third possible cause of the temperature difference variations is that the underlying assumption may not be strictly true, i.e. the two FOVs might actually be measuring differ-

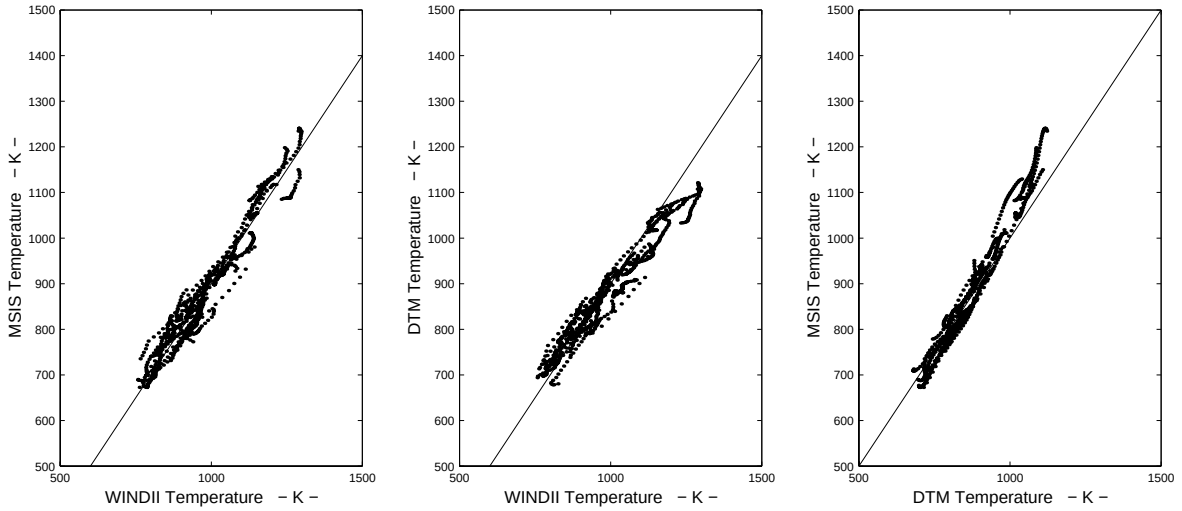

Fig. 7. Scattered plots showing the zonal mean temperatures for the 33 quiet days, averaged in the altitude range of 180 to 260 km, as given by the two empirical models and as measured by WINDII FOV1 (left and middle panels). The panel on the right shows the scattering between the two empirical models for comparison. Each point corresponds to a given latitude and points that are aligned belong to the same day.

ent average temperatures. This could result from a small, unanticipated horizontal structure in the temperature, since the two fields view the limb from different directions.

For the days studied, the background level is in the range of 0.5 to 5% of the ^{1}D signal, with an average of 1.5%. In the calculation of the background conversion factor, the standard deviation of the daily averages is about 0.3 of the average value, so a typical uncorrected background variation of $1.5\% \times 0.3 = 0.45\%$ of the ^{1}D signal could be expected. This corresponds to an uncertainty of 7 K in the apparent temperatures. It is interesting to note that the average of the daily $T1 - T2$ from Fig. 4 is also about 7 K. The worst case of 5% leads to a 24 K uncertainty. This is the maximum uncertainty to be expected from the background subtraction in the apparent temperature. As stated above, the variations in U are expected to be very small. Therefore, this value represents the maximum variation in the apparent temperature that we could expect from instrumental effects if, as we believe, these are the main sources of error. With a 24 K uncertainty due to instrumental effects and a 20 K mean random error value (i.e. the maximum value of the mean error plotted in Fig. 4), one obtains a standard deviation of 32 K, a value close to the maximum standard deviation of the daily apparent temperatures. Therefore, we consider that apparent temperature variations that are larger than this maximum value of the standard deviation are geophysical. Consequently, variations in the inverted temperatures greater than 40 K, the largest standard deviation in Fig. 5, can also be considered geophysically significant.

4 Comparison of temperature with empirical thermospheric models

The validation of the absolute value of the temperature requires comparison with other measurements. However, direct daytime measurements of the thermospheric temperature between 180 and 260 km do not currently exist. Ground-based interferometers are operated only during nighttime and incoherent scatter measurements do not provide direct measurements of the neutral temperature.

Earlier measurements of the daytime thermospheric temperature have been used to construct empirical models of the thermosphere and therefore, the comparison of our temperature with these models provides a way to check our data a posteriori.

Comparisons have been made with two empirical models: MSIS-90 (Hedin, 1991) and DTM-94 (Berger et al., 1998). Both models are based on data acquired during the earlier 1965–1983 period. MSIS-90 includes neutral temperature deduced from incoherent scatter measurements, while DTM-94 is based only on satellite measurements, primarily from DE-2 and OGO-6.

We have used the 33 O(^{1}D) quiet days of the WINDII database, i.e. corresponding to a daily A_p magnetic index equal to or smaller than 12. The temperatures from the models have been calculated at the local time, altitude, and geographical location of each FOV measurement, using the appropriate daily solar index F10.7 cm, as well as the A_p or K_p three-hourly magnetic indices. Then, WINDII temperatures and those from the model are averaged in the same way. Zonal means are calculated between the 180 and 260 km altitude and averaged in order to minimize the impact of oscillations observed on the WINDII temperature profiles. A daily mean temperature is also computed by averaging all latitudes. The daily mean temperatures are plotted as a function

of the UARS day in Fig. 6. The upper and lower panels show, respectively, the two FOV measurements. Here, they cannot be compared directly since unlike what we have done for the FOV comparison, we have not restricted the data set to the common portion of the orbit. The latitudinal coverage of the daytime measurements is, therefore, different for each FOV. The most important features of these plots are an excellent correlation coefficient of .97 and a bias of about 100 K between the models and the WINDII temperatures. The main time variation of the mean temperatures corresponds to the variation of the thermospheric temperature with solar activity, as shown by the plot of the solar flux F10.7 cm in the upper panel. The differences between the two models are very small apart from the early 1992 days, where they reach 80 K.

In Fig. 7, we show scatter plots of the WINDII temperatures retrieved from FOV1 measurements versus MSIS temperatures (left panel) and DTM temperatures (middle panel). This time, the latitudinal average has not been calculated. Each point corresponds, therefore, to a given latitude. Points which look aligned belong to the same day. This plot shows that the two models represent also very well the latitudinal/local-time variation observed in the WINDII data. The scatter is just a little larger than the scatter between the two models shown in the right panel. This last panel shows that the larger values of the model temperatures are different and the two first panels show that the largest values of WINDII temperatures are better represented by the MSIS model. The line drawn on the two first panels represents a bias of 100 K. In the last panel, we have just plotted the line of equal temperatures. The results are similar when one uses the WINDII measurements of FOV2.

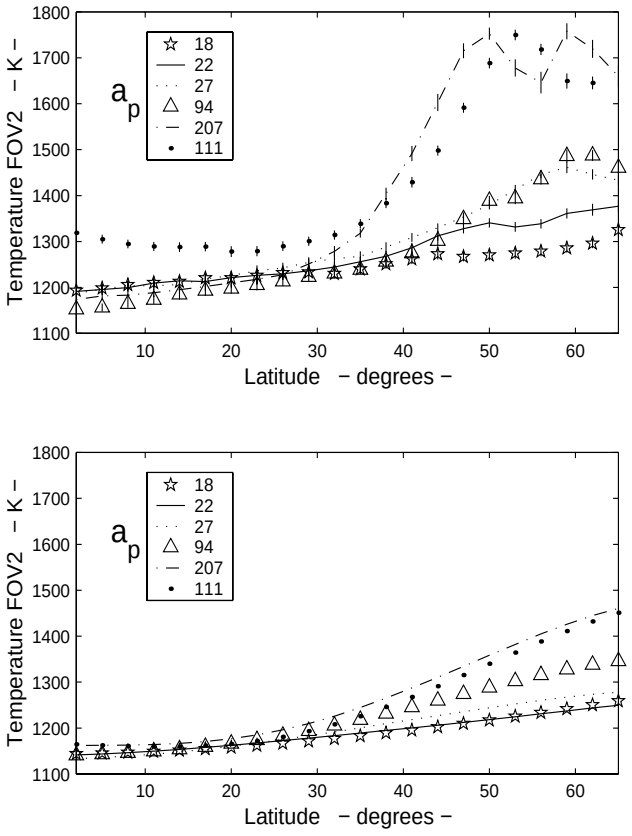

Fig. 8. Latitudinal/local time variations of the temperature for 6 orbits on UARS day 168. The temperatures for the different orbits are represented by different symbols, as indicated on the figure with the corresponding magnetic indices. The upper panel shows WINDII O(^{1}D) temperatures, while the bottom panel shows the MSIS-90 temperatures obtained at the same latitude/local time and for the same altitude range (220–260 km).

5 Example of temperature variations observed during a magnetically active day

All of the data used in our statistical analysis is the result of zonal means performed on magnetically quiet days. The main feature of the WINDII temperatures during disturbed days is their large variability from one orbit to another. An example is shown in the upper part of Fig. 8. Temperatures are plotted for 6 orbits of UARS day 168, i.e. 26 February 1992. Here, the averaging in altitude has been performed over the range of 220–260 km. The error bars are the averages of the measurement errors for the different altitudes. The local time of the observations varies from about 8 h at the equator to 11 h and 20 min at high-latitudes. This day corresponds to the largest daily A_p of our database: 68. The three-hourly A_p indices, corresponding to the 6 individual orbits, are indicated on the figure: they increase with UT from 18, to a maximum of 207 and decrease afterwards. One can observe a corresponding increase in the temperature, starting around 30° latitude for the highest A_p value. Orbit 6 has an A_p close to the one of orbit 4. However, its temperature is slightly smaller in comparison to that of orbit 5 and is still much larger than that of orbit 4. At low-latitude, the increase in temperature still occurs, but with a time delay of at least 3 hours. All of these features are well-known. For example, the temperature increase down to low-latitudes was already shown by Burns et al. (1995), using DE-2 satellite data. Such features can also be found in the empirical models, as shown on the lower panel. The main differences between the MSIS model and our data are quantitative: the magnitude of the increase is about two times larger in the WINDII data; the latitudinal variation of this increase is more dependent on the A_p magnitude in the WINDII data than in MSIS; and finally, the variation at low-latitudes is almost non-existent in the model. The comparison with DTM94, not shown here, is similar, with a somewhat smaller variation than in MSIS.

It is well-known that there are two major problems with the empirical models of the thermosphere: (1) magnetically disturbed days are poorly described since they do not capture the local and time variations of any particular storm or substorm, and (2) high-latitude regions are not well represented due to the sparseness of high-latitude data. These two features are very well documented. For example, Killeen et al. (1995) show that the temperature variations

with the solar cycle and with magnetic activity, observed by the Thule (Greenland) ground-based Fabry-Perot interferometer, have a much larger amplitude than MSIS variations. These variations will be investigated in greater detail using the O(^{1}D) WINDII data base.

6 Discussion

The WINDII O(^{1}D) temperatures, as given by version 5.11 of the software, are about 100 K higher than the empirical thermospheric temperatures. Three possible explanations will be successively discussed: the inadequacy of empirical models of the current thermospheric temperatures, the presence of non-thermal O(^{1}D) atoms, and finally, an error in the instrument's visibility calibration.

As we have outlined above, the empirical models do not accurately represent the temperature variations associated with magnetic activity for a given day. However, it is usually an accepted fact that they give a good statistical representation of the magnetically quiet mid-latitude thermosphere. Therefore, the question arises as to whether the whole bias or part of the bias observed between WINDII and the models could be an indication of the existence of a long-term trend in the thermospheric temperature. Buonsanto and Pohlman (1998) have presented a comprehensive study of the exospheric temperature at Millstone Hill, using 201 days of observations between 1981 and 1997. They found a good agreement between the climatology deduced from their observations, the previous Millstone Hill climatologies and the MSIS model, and could not find any significant long-term trend in their data set. Therefore, we conclude that the observed 100 K bias in our data cannot be explained in this way.

With the radiative lifetime of O(^{1}D) atom at about 107 s (Fischer and Saha, 1983), its thermalization at high altitudes may not be completely effective. Using a simple model, Schmitt et al. (1981) have interpreted an excess of the 6300 Å intensity above 600 km as evidence of nonthermal O(^{1}D) atoms. In 1999, Shematovich et al. have reported their studies of thermalization with a Monte Carlo model and predicted an excess O(^{1}D) temperature of 350 K at noon for low solar activity conditions at the altitude of 300 km. For high solar activity conditions, the thermalization is more effective. They have concluded that the temperatures deduced from airglow observations may exceed the ambient gas temperature depending not only on solar activity and local time, but also on the observation geometry. In a more recent paper, Hubert et al. (2001) found that the observations by the DE-2 Fabry-Perot interferometer of temperatures much higher than the MSIS model could be a possible signature of nonthermal O(^{1}D) atoms. They show that the downward propagation of high altitude non-thermal effects on the line shape through limb inversion could explain an overestimation of 100 to 150 K above the MSIS model in part of the observations. However, considering the differences between the two types of measurements and their inversion schemes, this argument does not apply to WINDII measurements. This is further supported by the fact that (as shown in Fig. 9) we do not seem to find any clear variation of this observed bias with solar activity as would otherwise be expected (Shematovich et al.,1999): Fig. 9 shows the differences between MSIS and WINDII mean temperatures (in the altitude range of 180–260 km) as a function of the F10.7 cm index. An alternative possibility is that one or more of the source constituents may itself not be in the neutral state, contrary to what is currently assumed in O(^{1}D) thermalization studies.

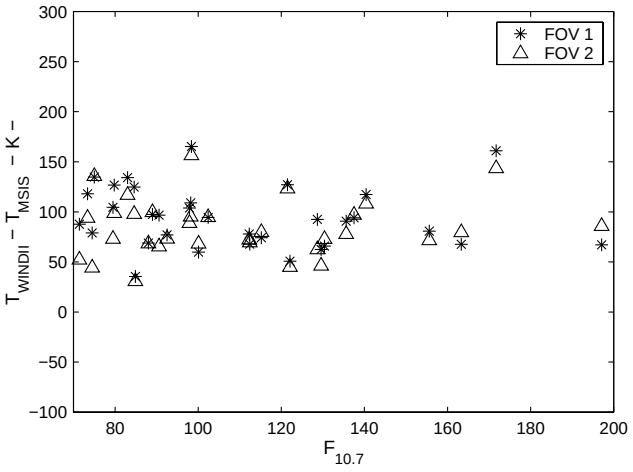

Fig. 9. Differences between the mean daily temperatures observed by WINDII and given by the MSIS-90 empirical model for the quiet days as a function of the solar activity.

The last point we have to mention is the possibility of an error during the instrumental visibility calibration. A 5% error in this calibration will result in a 80 K bias on measured temperatures. This value is an upper limit on the possible error in the instrumental visibility on the one hand, and on the other hand, great precautions have been taken during preflight calibrations to limit such problems and we believe such a large error is unlikely. However, we cannot yet rule out the possibility that an instrument visibility calibration error contributes to the bias.

7 Conclusion

Daytime O(^{1}D) Doppler temperatures have been retrieved from WINDII measurements during the first four years of observation. We have shown that observations of the two WINDII FOVs give temperatures that statistically differ by less than 20 K and that variations greater than 40 K can be considered geophysically significant. We have shown that the latitudinal/local time variations and the solar cycle variation of the zonal means for magnetically quiet days is in excellent agreement with the MSIS-90 and DTM-94 empirical models. We have also shown an example of temperature variations between successive orbits during a very disturbed day that are qualitatively in agreement with the models. The study of such variations associated with magnetic activity,

Table A1. Interferometric Parameters for O^1D and O^1S

Parameter	$O^1S(630.0\,\mathrm{nm})$	$O^1S(557.7\,nm)$	Units
Q	$2.87\cdot10^{-5}$	$3.66\cdot10^{-5}$	$\mathrm{K}^{-1}\,\mathrm{cm}^{-2}$
Δ_0	4.4687	4.4865	cm
$\partial\Delta/\partial\lambda$	−2109	−2884	
D	4.6015	4.6473	cm

Table A2. Temperature error produced by using Δ_0 instead of D

Emission	Path difference error, $\delta D/D$	Temperature, T K	Temperature error, δT K
^1D	3.0%	800	48
		1200	72
		1600	96
^1S	3.6%	200	14

using the complete O(^{1}D) WINDII data base, will be the object of a further study.

We have, however, to face two major problems: the presence of oscillations in the tangent altitude temperature profiles, thus leading us to work with altitude averages, and a bias of about 100 K between the Doppler temperatures and the empirical models. These two problems need to be investigated further. One of the available avenues is a comparison with lower altitude temperatures derived from the WINDII O(^{1}S) emission.

Appendix A The path difference and its influence on the temperature value

In the first versions of the WINDII processing software, the Doppler temperature has been calculated from Eq. (2) using the form

$$V = \exp -QT\Delta_0^2, \tag{A1}$$

where Δ is the simple path difference given by $\Delta = 2(n_1t_1 + n_2t_2 + t_3)$ and the subscript "0" refers to the wavelength of the emission line centre. Here, t_1 and t_2 are the length of the interferometer's glass arms and n_1 and n_2 are the respective refractive indices, and t_3 is the length of the gap in front of the moving mirror. As Thuillier and Hersé (1991) pointed out, it is important to include the dependence of the path difference on the wavelength when calculating the wind, and it was suggested by Thuillier (Personal communication, 1988) that this effect might also be important in calculating the Doppler temperature. Here, we show that it is indeed necessary to include the dispersion of the path difference in an accurate calculation of the Doppler temperature.

The intensity, I, in the interferogram produced by a Gaussian emission line of width w is

$$I = I_0\sqrt{\frac{4\ln 2}{\pi w^2}}\int_{-\infty}^{\infty}\exp\left(\frac{4\ln 2}{\pi w^2}(\sigma-\sigma_0)^2\right)\big(1+\cos 2\pi\Delta\sigma\big)d\sigma, \tag{A2}$$

where σ is wave number, σ_0 is the wave number of the emission line centre, and I_0 is the average line intensity.

Assuming that the dispersion of the path difference is linear across the width of the emission line, we can write

$$\begin{aligned}\Delta\sigma &= \left(\Delta_0 + (\lambda-\lambda_0)\frac{\partial\Delta}{\partial\lambda}\right)\sigma\\ &= \left(\Delta_0 - \lambda_0\frac{\partial\Delta}{\partial\lambda}\right)(\sigma-\sigma_0+\sigma_0) + \lambda\frac{\partial\Delta}{\partial\lambda}\sigma\\ &= \left(\Delta_0 - \lambda_0\frac{\partial\Delta}{\partial\lambda}\right)(\sigma-\sigma_0)\\ &\quad + (-\lambda_0\sigma_0 + \lambda\sigma)\frac{\partial\Delta}{\partial\lambda} + \Delta_0\sigma_0\\ &= \left(\Delta_0 - \lambda_0\frac{\partial\Delta}{\partial\lambda}\right)(\sigma-\sigma_0) + \Delta_0\sigma_0\\ &= D(\sigma-\sigma_0) + \Delta_0\sigma_0.\end{aligned} \tag{A3}$$

Here, the quantity $D = \Delta_0 - \lambda_0(\partial\Delta/\partial\lambda)$ is the effective path difference first identified by Thuillier and Hersé (1991) in reference to the wind calculation. Replacing Eq. (A3) in Eq. (A2), we have

$$\begin{aligned}I &= I_0\sqrt{\frac{4\ln 2}{\pi w^2}}\int_{-\infty}^{\infty}\exp\left(\frac{-4\ln 2}{w^2}(\sigma-\sigma_0)\right)\\ &\qquad [1+\cos 2\pi\Delta_0\sigma_0\cdot\cos 2\pi D(\sigma-\sigma_0)]\,d\sigma\\ &= I_0\left\{1+\exp\left(-\frac{2\pi^2k\sigma_0^2}{mc^2}D^2T\right)\cos 2\pi\Delta_0\sigma_0\right\}\end{aligned} \tag{A4}$$

(The integral of the sine term is not shown; it is zero due to antisymmetry.) The exponential factor in Eq. (A4) is the emission line visibility, $V = \exp(-QD^2T)$, where $Q = 2\pi k\sigma_0^2/(mc^2)$, k is Boltzman's constant, and m is the atomic mass. This uses the effective path difference, D, rather than the simple path difference. Values for Q, Δ_0, and D are given in Table A1 for the WINDII interferometer and for the two emissions used to calculate Doppler temperature; Δ_0 and D were calculated from the interferometer's arm lengths and the glass properties were supplied by the manufacturer.

For the ^1D emission, D is 3.0% greater than Δ_0 and for ^1S, it is 3.6% greater. From Eq. (2)

$$T = -\frac{\ln V}{QD^2} \tag{A5}$$

so a given measured value of V gives a temperature that is too high if Δ_0 is used instead of D. By differentiating Eq. (A2) with respect to T, we obtain

$$\delta T \cong -\frac{1}{QD^2} \cdot \frac{\delta V}{V}, \tag{A6}$$

where δT is the temperature error caused by a relative change $\delta V/V$ in the visibility. Similarly, differentiating with respect to D gives $\delta V/V \cong -2QTD\delta D$, and combining this with (A6) gives

$$\delta T \cong 2T\frac{\delta D}{D}, \tag{A7}$$

where $\delta D/D$ is the relative error in D. The approximations are valid for $\delta D/D < 0.1$. The temperature errors caused by the use of δ_0 in versions of the data processing software before 5.11 are given in Table A2 for selected temperatures. The temperatures in the earlier versions are too high by the amounts shown in the last column.

Acknowledgement. Discussions with G. Thuillier, F. Vial and G. Shepherd are gratefully acknowledged. This work has been supported by CNES and by the Canadian Space Agency. One of the authors (W. Gault) received a bursary from le Ministère de l'Education Nationale, de la Recherche et de la Technologie (France).

Topical Editor M. Lester thanks two referees for their help in evaluating this paper.

References

Berger, C., Biancale, R., YII, M., and Barlier, F.: Improvement of the empirical thermopsheric model DTM: DTM94 - a comparative review of various temporal variations and prospects in space geodesy applications, J. Geodesy, 72, 161–178, 1998.

Buonsanto, M. J. and Pohlman, L. M.: Climatology of neutral exospheric temperature above Millstone Hill, J. Geophys. Res., 103, 23 381–23 392, 1998.

Burns, A. G., Killeen, T. L., Deng, W., Carignan, G. R., and Roble, R. G.: Geomagnetic storm effects in the low to middle upper thermosphere, J. Geophys. Res., 100, 14 673–14 691, 1995.

Fischer, C. F. and Saha, H. P.: Multi-configuration Hartree-Fock results with Breit-Pauli corrections for forbidden transitions in the 2p4 configuration, Phys. Rev. A., Gen. Phys., 28, 3169–3178, 1983.

Gault, W. A., Lathuillère, C., and Rochon, Y. J.: Measuring thermospheric temperatures with WINDII, Internal report, Laboratoire de Planétologie de Grenoble, France, 1999.

Gault, W. A., Thuillier, G., Shepherd, G. G., Zhang, S. P., Wiens, R. H., Ward, W. E., Tai, C., Solheim, B. H., Rochon, Y. J., McLandress, C., Lathuillère, C., Fauliot, V., Hersé, M., Hersom, C. H., Gattinger, R., Bourg, L., Burrage, M. D., Franke, S. J., Hernandez, G., Manson, A., Niciejewski, R., and Vincent, R. A.: Validation of O(^{1}S) wind measurement by WINDII: the wind imaging interferometer on UARS, J. Geophys. Res., 101, 10 405–10 430, 1996.

Hedin, A. E.: Extension of the MSIS thermosphere model into the middle and lower thermopshere, J. Geophys. Res. 96, 1159–1172, 1991.

Hubert, B., Gérard, J. C., Killeen, T. L., Wu, Q., Bisikalo, D. V., and Shematovich, V. I.: Observation of anomalous temperatures in the daytime O^{1}D 6300 A thermospheric emission: a possible signature of nonthermal atoms, J. Geophys. Res., 12 753–12 764, 2001.

Killeen, T. L., Won, Y. I., Niciejewski, R. J., and Burns, A. G.: Upper thermospheric winds and temperatures in the geomagnetic polar cap: Solar cycle, geomagnetic activity, and interplanetary magnetic field dependencies, J. Geophys. Res., 100, 21 237–21 342,1995.

Lathuillère, C., Lilensten, J., Gault, W., and Thuillier, G.: The meridional wind in the auroral thermosphere: results from EISCAT and WINDII O^{1}D coordinated measurements, J. Geophys. Res., 102, 4487–4492, 1997.

Rochon, Y. J.: The retrieval of winds, Doppler temperatures and emission rates for the WINDII experiment, PhD Thesis, York University, Toronto, Canada, 2000.

Schmitt, G. A., Abreu, V. J., and Hays, P. B.: Non thermal O(^{1}D) produced by dissociative recombination of O2+: a theoretical model and observed results, Planet. Space Sci., 29, 1095–1099, 1981.

Shematovitch, V. I., Gerard, J. C., Bisikalo, D. V. and Hubert, B.: Thermalization of O(^{1}D) atoms in the thermosphere, J. Geophys. Res., 104, 4287–4295, 1999.

Shepherd, G. G., Thuillier, G., Gault, W. A., Solheim, B. H., Hersom, C., Brun, J.-F., Charlot, P., Desaulniers, D.-L., Evans, W. F. J., Girod, F., Harvie, D., Llewellyn, E. J., Lowe, R. P., Powell, I., Rochon, Y., Ward, W. E., Wiens, R. H., and Wimperis, J.: WINDII the Wind Imaging Interferometer on the Upper Atmopshere Research Satellite, J. Geophys. Res., 98, 10 725–10 750, 1993.

Thuillier, G. and Hersé, M.: Thermally stable field compensated Michelson interferometer for measurement of wind of the planetary atmospheres, Appl. Optics, 30, 1210–1220, 1991.

Thuillier G., Fauliot, V., Hersé, M., Bourg, L., and Shepherd, G. G.: The MICADO wind measurement from Observatoire de Haute-Provece for the validation of the WINDII green line data, J. Geophys. Res., 101, 10 431–10 440, 1996.

Thuillier, G., Gault, W. A., Brun, J.-F., Hersé, M., Ward, W., and Hersom, C.: In flight calibration of the WINDII interferometer onboard the UARS satellite, Appl. Optics, 37, 1356–1369, 1998.